

A computational homogenization framework for soft elastohydrodynamic lubrication

M. Budt · İ. Temizer · P. Wriggers

Received: 22 September 2011 / Accepted: 21 March 2012 / Published online: 28 April 2012
© Springer-Verlag 2012

Abstract The interaction between microscopically rough surfaces and hydrodynamic thin film lubrication is investigated under the assumption of finite deformations. Within a coupled micro–macro analysis setting, the influence of roughness onto the macroscopic scale is determined using FE^2 -type homogenization techniques to reduce the overall computational cost. Exact to within a separation of scales assumption, a computationally efficient two-phase micromechanical test is proposed to identify the macroscopic interface fluid flux from a lubrication analysis performed on the deformed configuration of a representative surface element. Parameter studies show a strong influence of both roughness and surface deformation on the macroscopic response for isotropic and anisotropic surficial microstructures.

Keywords Reynolds equation · Surface roughness · Homogenization · Finite deformation

Nomenclature

β Angle of orientation w.r.t. x-axis
 \bullet^S Surface quantities
 $\bullet^{+/m/-}$ Quantities belonging to the upper-, middle-, lower-surface of the fluid element, respectively ($m \leftarrow p, q$)

$\mathcal{L}, \partial\mathcal{L}$ Fluid domain and its boundary in current configuration
 $\mathcal{S}, \partial\mathcal{S}$ Solid domain and its boundary in current configuration
 ϵ_C Parameter to penalize the fluid pressure to p_a
 $\langle \bullet \rangle$ Surface averaged local quantities
 $\bar{\bullet} = \langle \bullet \rangle$ Macroscopic quantities
 F/H Surface deformation/displacement gradient
 n^\bullet Fluid normal vectors on surfaces +, m, -
 q Fluid flux per density
 q^c Fluid flux Couette term
 q^p Fluid flux Poiseuille term
 a Deformed surface area
 A_0 Undeformed surface area
 p Fluid pressure
 p_a Bearing surrounding ambient pressure
 \dot{v} Fluid acceleration
 α Pressure–viscosity coefficient
 $\eta^p, \eta^{g/u}$ Test function w.r.t. p, g or u
 \bar{v} Rel. surface velocity
 μ_0 Dynamic viscosity
 ρ Density
 b Body force
 g Grad[p] pressure gradient
 v Fluid velocity
 h Gap height
 l_z Sample height z
 $l_{x,y}$ Gap/sample length x, y
 ν Poisson's ratio
 Ψ Strain energy function
 E Young's modulus
 G Shear modulus
 K Bulk modulus
 U Volumetric part of strain energy function

M. Budt (✉) · P. Wriggers
Institute of Continuum Mechanics, Leibniz University
of Hanover, Appelstr. 11, 30167 Hannover, Germany
e-mail: budt@ikm.uni-hannover.de

İ. Temizer
Department of Mechanical Engineering, Bilkent
University, 06800 Ankara, Turkey

1 Introduction

In many cases of engineering interest, two surfaces that appear to be macroscopically in contact are separated by a thin fluid film on the microscale. The presence of such a film may be desirable or undesirable. The synovial fluid is critical to the healthy functioning of human joints [21] and lubricants are an integral design parameter in order to maintain the operation standards in various machinery by minimizing wear [38]. On the other hand, wet road surfaces may lead to poor tire traction performance and eventually to hydroplaning [19] while oil, a common lubricant, can also lead to reduced performance in wheel-rail contact [31]. An investigation of the tribological nature of such surfaces is an interdisciplinary task that forms the basis of the lubrication theory. See Hamrock et al. [22], Persson [36], Szeri [51] for extensive overviews of the field.

A central ingredient of the lubrication theory is the REYNOLDS equation [40] that is derived from the three-dimensional Navier–Stokes equations in the thin film limit. The REYNOLDS equation enables a predictive analysis of lubricated interfaces over a broad range of macroscopic contact situations and therefore plays a fundamentally practical role in circumventing a direct solution of the computationally more challenging Navier–Stokes equations. However, in its original form, the REYNOLDS equation assumes microscopically flat surfaces and employing a mean film thickness together with the original equation is generally unable to capture roughness effects accurately. Consequently, the construction of robust techniques of incorporating the effects of tribologically realistic surfaces that display roughness at various scales into the REYNOLDS equation has been of prime interest, in particular for surface texture design applications [52]. For the purposes of this work, attempts towards this goal may be grouped into two major categories: (i) stochastic approaches that augment the original REYNOLDS equation and (ii) homogenization techniques. The widely employed influential works of Patir and Cheng [34] and Patir and Cheng [35] introducing the flow factor method belong to the former category. Additional early works of historical interest include Tripp [57] where anisotropic texture effects were accounted for and Shukla [47] where an effective viscosity concept was introduced. For recent references, the reader is referred to Hamrock et al. [22] and Szeri [51].

Parallel to these efforts were perturbation techniques that operated directly on the fine scale pressure oscillations—see Tripp [57] for an early approach and Persson [37] for a recent development. Among these, the small-parameter expansion approach of Elrod [18] can be considered as a precursor to modern homogenization techniques in lubrication and shows similarities with the asymptotic expansion treatments that were first initiated in the context of heterogeneous media [5, 9, 44]—see Fabricius [20] for a review.

For heterogeneous materials and interfaces, the homogenization approach based on the asymptotic expansion technique is exact in the sense that the macroscopic response of the medium can be extracted based on a given microstructure and microscale constitutive models without further simplification. Moreover, this inherently multiscale approach lends itself to computational homogenization frameworks (often referred to as FE^2) which can operate in periodic and random multiphysics settings, with discrete media or under constraint conditions like contact and in particular at finite deformations where analytical or closed-form mathematical approaches pose difficulties. While these advantages are at the expense of significant computational cost, their predictive potential complements and in some cases supersedes the alternatives offered by approximate homogenization techniques, such as estimates and bounds, based on simplified microstructures and constitutive relationships which are usually necessary to enable an analytical treatment of the multiscale problem. See Stupkiewicz [49], Temizer [53], Temizer and Wriggers [55], Torquato [56], Zohdi and Wriggers [61] for overviews with extensive references on computational homogenization techniques and their applications to finite deformation problems for materials and interfaces.

Asymptotic expansion based approaches have been analyzed for the REYNOLDS equation with and without cavitation, in the presence of compressibility effects as well as a possibly non-Newtonian fluid in various works. Recent examples include Almqvist and Dasht [1], Almqvist et al. [2, 3], Bayada et al. [7], Jai and Bou-Said [26], Kane and Bou-Said [27, 28]—see also references therein for further remarks on the historical development of the approach. These enable exact treatments of the multiscale problem and are amenable to a computational implementation, thereby circumventing the demanding task of resolving microscopic roughness directly in the solution of the macroscopic problem, cf. Fig. 1. Recently, analytical bounds for the macroscopic lubrication behavior have also been derived [4, 32], which are closely related to the bounds for heterogeneous materials [56]. Such bounds deliver a solution space for the performance of hydrodynamic lubrication as influenced by real measured surface roughness. Recent comparisons of homogenization and flow factor approaches may be found in Sahlin et al. [41–43]. As for heterogeneous media, absolute length scale dependence is also of concern in lubrication [24]. However, such effects are outside the scope of the present study.

All of the investigations to be performed in this study employ microstructures that may be classified as being in the REYNOLDS roughness regime, together with gap heights where roughness effects are significant. The roughness classification goes back to the work of Elrod [18] and verifies the assumption regarding the validity of the REYNOLDS equation

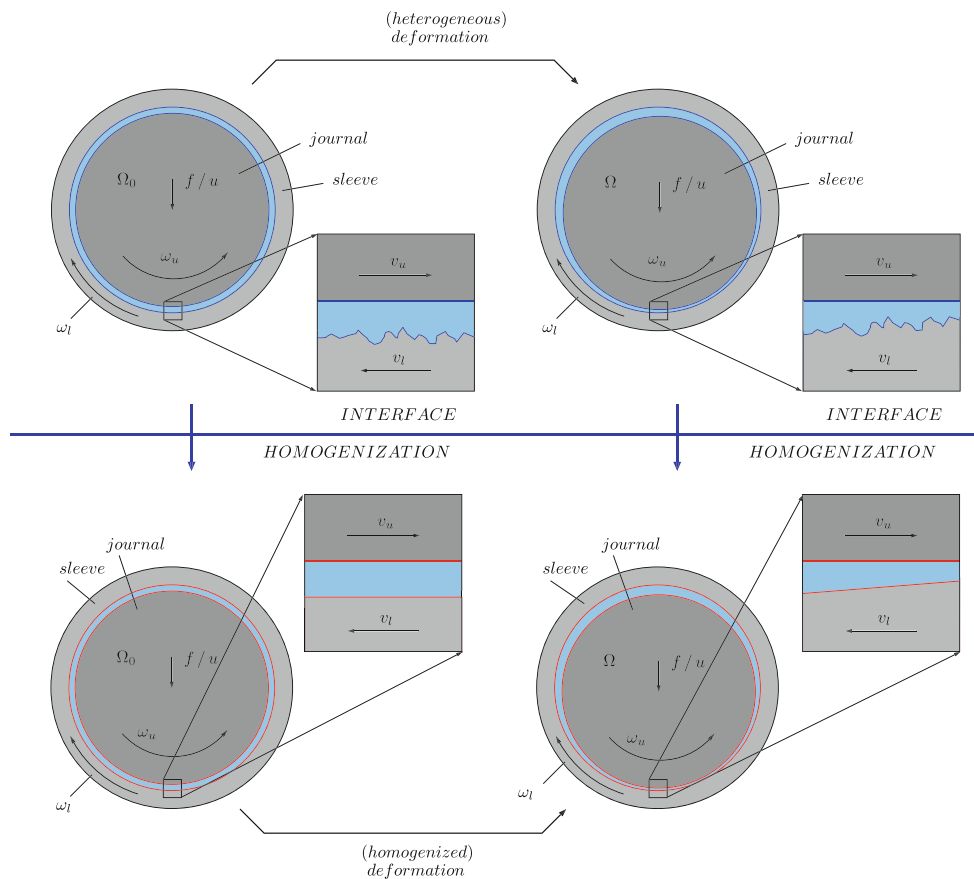


Fig. 1 The lubrication homogenization idea is summarized. The original non-smooth boundary topography of the deformable body is replaced with a microscopically smooth one, leading to a homogenized problem with a lower discretization cost

on the microscale within the micromechanical analysis. The investigations of Mitsuya and Fukui [33] indicate that, the roughness wavelength to mean film thickness ratio should be approximately five or larger if this assumption to hold. Otherwise, the Stokes roughness regime becomes dominant and a direct solution of the Stokes equation is suggested, although alternative limit equations have also been obtained in the mathematical literature [6]. In the case of dynamic effects, a reversion to the original Navier–Stokes equation may be required within the homogenization framework, which may also be necessary in the case of near-contact situations where the gap height to combined roughness ratio is very small [16]. In the other extreme of this ratio, roughness effects are negligible. They become dominant in the vicinity of a gap to combined roughness ratio of the order of ten and below [34].

The major goal of this work is to introduce and investigate a computational homogenization framework for soft, i.e. finite deformation, elastohydrodynamic lubrication. The multiscale problem in the context of elastohydrodynamic lubrication has been investigated in Bayada et al. [8], Bohan et al. [10], Dowson [17] and explicit numerical

solution strategies for the coupled problems of elasticity and lubrication have been proposed [29]. Although finite deformation effects have also been investigated in Shi and Salant [45], Shinkarenko et al. [46], Stupkiewicz and Maciniszyn [50], a sufficiently general computational homogenization framework that takes into surface texture evolution effects due to large macroscopic deformations of the lubricated interface appears not to have been proposed. With a view towards establishing such a framework, Sect. 2 introduces the macroscopic soft elastohydrodynamic lubrication analysis framework in the context of the finite element method. A sample problem is additionally analyzed to motivate the multiscale computational homogenization framework. Subsequently, Sect. 3 constructs the homogenization methodology. In addition to a discussion of scale transition procedures, thermodynamical consistency of the proposed formulation is discussed by monitoring dissipation on micro- and macroscales. Finally, major aspects of the proposed approach are demonstrated in Sect. 4 with an emphasis on finite deformation effects and the associated macroscopically anisotropic interface flow considerations.

2 Lubrication problem

2.1 REYNOLDS equation

The starting point for interface flow considerations is the mass balance together with the Navier–Stokes equations. The former is taken into account by the continuity equation statement [22, 59]. The NAVIER–STOKES equations can be derived from the differential volume element and capture fluid behaviour in general. The fluid flux of the steady state REYNOLDS equation (2.21) is derived from the NAVIER–STOKES equations under certain assumptions:

- (i) body forces and inertia effects are negligible,
- (ii) thin channel fluid flow, bounded by two surfaces in relative motion,
- (iii) perfect stick of fluid molecules on solids,
- (iv) no fluid flow (velocity) across the fluid channel,
- (v) negligible pressure change across the fluid channel,
- (vi) Newtonian fluid,
- (vii) incompressible fluid.

Defining the fluid flux

$$\mathbf{q} = \underbrace{-\frac{h^3}{12\mu} \mathbf{g}}_{\mathbf{q}^p} + \underbrace{\frac{h\bar{\mathbf{v}}}{2}}_{\mathbf{q}^c} \quad (2.1)$$

the Reynolds equation with boundary conditions can be stated as $(\partial\mathcal{L}^p \cup \partial\mathcal{L}^q = \partial\mathcal{L})$

$$\begin{aligned} &-\rho \operatorname{div}[\mathbf{q}] = 0 \text{ in } \mathcal{L} \\ \text{subject to } &p = \hat{p} \text{ on } \partial\mathcal{L}^p \\ &\text{and } -\mathbf{q} \cdot \mathbf{n} := \hat{q}_n \text{ on } \partial\mathcal{L}^q \end{aligned} \quad (2.2)$$

Here, the constitutive dependence $\mathbf{q} = \mathbf{q}(h, p, \mathbf{g}, \bar{\mathbf{v}})$ holds where p is the fluid pressure and $\mathbf{g} = \operatorname{grad}[p]$ its gradient, $\bar{\mathbf{v}}$ is the relative tangential velocity between the adjacent surfaces and h is the distance between those surfaces (see also Fig. 5). Here the lower surface is stationary and the gap height varies little along the x and y directions. For future reference, the flux has also been additively decomposed as $\mathbf{q} = \mathbf{q}^p + \mathbf{q}^c$ into the Poiseuille term \mathbf{q}^p which depends nonlinearly on the pressure p and the linear COUETTE term \mathbf{q}^c . Within the Poiseuille term, the nonlinearity arises from $\mu(p) = \mu_0 \cdot e^{\alpha p}$, namely Barus equation holds. The dynamic viscosity μ_0 has to be chosen for a reference temperature. For water and low working pressures the pressure–viscosity coefficient α remains zero [48, p. 21, Table 2.3]. It is remarked that the derivation of the REYNOLDS equation was recently revisited in Rajagopal and Szeri [39] with a pressure dependent viscosity and an augmented formulation was obtained. Nevertheless, the commonly accepted convention of employing

Barus viscosity in the classical equation is followed in the present work.

2.2 Elastohydrodynamic framework

The contribution of the lubrication formulation to the weak formulation of the coupled problem in an elastohydrodynamic framework reads

$$\begin{aligned} I_{lubr} = & \underbrace{\int_{\mathcal{L}^p} \mathbf{q} \cdot \boldsymbol{\eta}^s \, da}_{I_F :=} + \underbrace{\int_{\partial\mathcal{L}^q} \begin{matrix} 0, \text{ on } \partial\mathcal{L}^p \\ \hat{q}_n \boldsymbol{\eta}^n \end{matrix} dl}_{I_C :=} \\ & - \int_{\mathcal{L}^{u^-}} p \mathbf{n}^- \cdot \boldsymbol{\eta}^u \, da - \int_{\mathcal{L}^{u^+}} p \mathbf{n}^+ \cdot \boldsymbol{\eta}^u \, da \\ & + \underbrace{\int_{\mathcal{L}^p} \eta^p \epsilon_C \{p - p_a\} \, da}_{I_{Cav} :=} \end{aligned} \quad (2.3)$$

where I_F and I_C denote the fluid (REYNOLDS equation 2.1) and fluid–solid coupling terms, respectively, and ϵ_C is a sufficiently large penalty parameter. Both terms are functions of the surface displacements \mathbf{u} and pressure p . Due to the nonlinear dependence on pressure in Eq. (2.3) and a finite deformation regime for the solids, the solution of the coupled problem requires the linearization of both the fluid and the contact contributions. Moreover, in order to take into account the effect of cavitation, the fluid pressure may not drop below the ambient pressure. Therefore, two conditions are distinguished, cf. Wriggers [60]:

1. no cavitation: $p - p_a \geq 0 \Rightarrow \epsilon_C = 0 \Leftrightarrow I_{Cav}$ is not computed,
2. cavitation: $p - p_a < 0 \Rightarrow \epsilon_C \gg 0 \Leftrightarrow I_{Cav}$ must be computed.

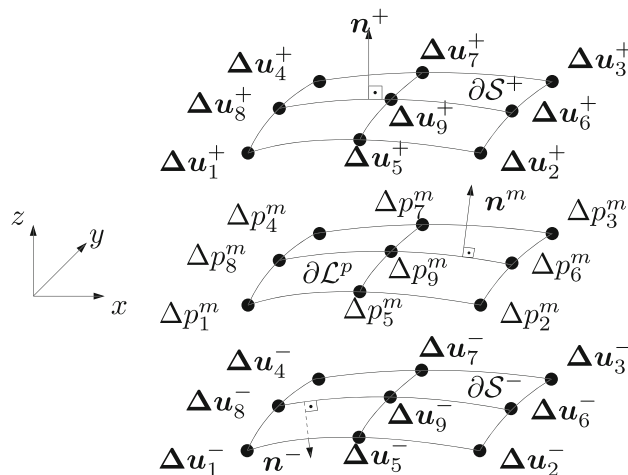


Fig. 2 Finite element with additional midsurface nodes

Table 1 Material parameters employed in Sect. 2 are summarized

Sleeve (Neo Hook)			
Young’s modulus (N/mm ²)	E		475.0
Poisson’s ratio	ν		0.499
Cylinder dimensions (mm)	$\varnothing^o \times \varnothing^i \times \text{width}$		490 × 451 × 375
Number of quadratic elements	$\varnothing^o \times \varnothing^i \times \text{width}$		80 × 24 × 3
Journal			
Young’s modulus (N/mm ²)	E		50000.0
Poisson’s ratio	ν		0.3
Cylinder dimensions (mm)	$\varnothing^o \times \varnothing^i \times \text{width}$		450 × 240 × 375
Number of quadratic elements	$\varnothing^o \times \varnothing^i \times \text{width}$		80 × 24 × 2
y-displacement (mm)			0.63
Lubricant (Water)			
Rel. vel. (journal–sleeve) (mm/s)	\bar{v}		2356.0
Viscosity (at 20 °C) (MPa s)	μ		1.0×10^{-9}
Pressure–viscosity coefficient (Pa ⁻¹)	α		0.0
Ambient-pressure (MPa)	\bar{p}_a		0.1
Cavitation penalty parameter (MPa)	ϵ_C		$1.0e^{12}$
Number of quadratic elements	$\varnothing^o \times \varnothing^i \times \text{width}$		80 × 24 × 1

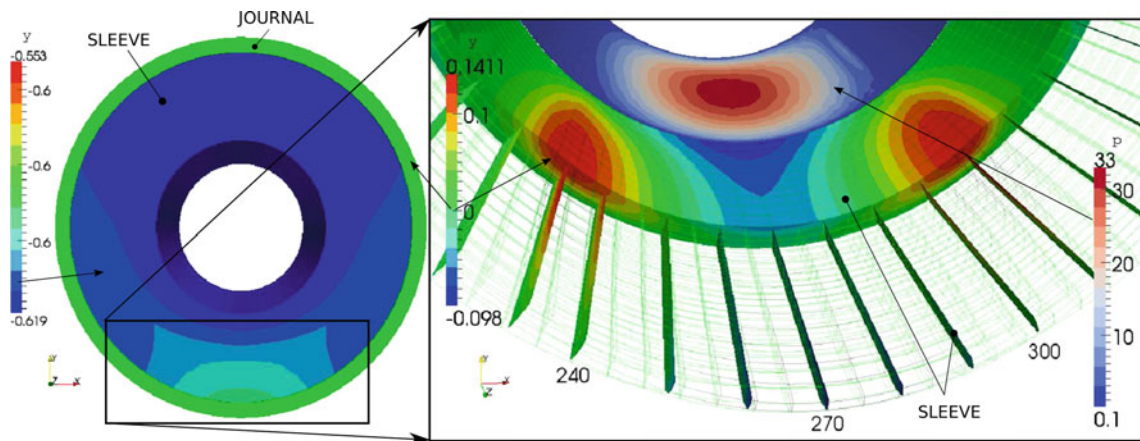


Fig. 3 Journal bearing macroscopic pressure \bar{p} and y-displacement plot. *left figure* Side view on journal bearing. Journal displacement in negative y-direction (blue colors) is shown. Sleeve (uniform green

colored) remains stationary. *right figure* Close up view on sleeve y-displacement (foreground) scaled by a factor of ten, caused by pressure p . This pressure distribution is shown in the background

Within a finite element framework which employs quadratic elements at the interface [15, 23], the displacement values are stored in the upper and lower plane nodes as depicted in Fig. 2. Here, the three dimensional interface elements represent the two dimensional curvilinear surficial problem of lubrication, cf. Wagner and Gruttmann [58, p. 153]. The lubrication pressure is stored in the additional middle nodes (Fig. 2). The coupling between the solid and the lubricant is carried out via the normals on the surfaces, which prescribe the direction in which the fluid pressure acts as a surface load.

The constitutive equation used for the incompressible rubber material of the sleeve is derived from a Neo-Hookean type strain energy function with the volumetric-deviatoric decoupling

$$\Psi = \left(K - \frac{2}{3}G \right) U(J) + \frac{1}{2}G(\text{tr}[C] - 3),$$

$$U(J) = J^2 - 1 - 2 \ln[J]$$

$$K = \frac{E}{3(1 - 2\nu)}, \quad G = \frac{E}{2(1 - \nu)}, \quad (2.4)$$

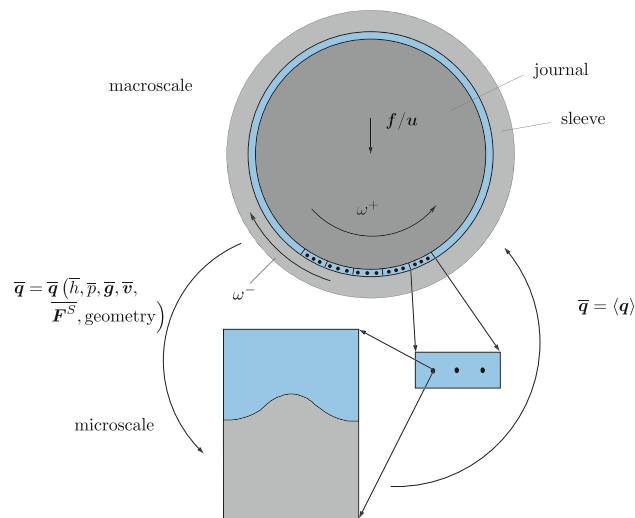


Fig. 4 Micro–macro loop with parameter interface between macroscale to micromechanical test procedure

where $J = \det[\mathbf{F}]$, with \mathbf{F} as the deformation gradient, $\mathbf{C} = \mathbf{F}^T \mathbf{F}$, K and G are the bulk and shear moduli, E is the Young's modulus and ν is the Poisson's ratio. The corresponding boundary value problem reads

$$\begin{aligned} \operatorname{div}[\boldsymbol{\sigma}] + \mathbf{b} &= 0 \quad , \text{ in } \Omega \\ \text{subject to } \mathbf{u} &= \bar{\mathbf{u}} \quad , \text{ on } \Gamma^u \\ \text{and } \mathbf{t} = \boldsymbol{\sigma} \cdot \mathbf{n} &= \bar{\mathbf{t}} \quad , \text{ on } \Gamma^\sigma. \end{aligned} \quad (2.5)$$

Here $\boldsymbol{\sigma}$ denotes the CAUCHY stress, \mathbf{b} is the body force, $\bar{\mathbf{u}}$ represents the displacement on Γ^u . Further $\bar{\mathbf{t}}$ prescribes traction on Γ^σ and note that Γ^σ includes the lubrication interface where $\bar{\mathbf{t}} = \boldsymbol{\sigma} \cdot \mathbf{n} = -pn$ holds, see Eq. (2.3). In order to demonstrate the framework, subject to input parameters in Table 1, a computational result is shown in Fig. 3.

3 Lubricant homogenization methodology

3.1 Interface testing procedure

Solving the REYNOLDS equation for a macroscale lubrication problem while taking into effect surfacial microscopic roughness that is several orders of length scales smaller demands a very fine mesh resolution and hence prohibitive computational times. To reduce the workload, a homogenization scheme is introduced. The basic idea is outlined in Fig. 4, where a mass balance

$$-\rho \operatorname{div}[\bar{\mathbf{q}}] = 0 \quad (3.1)$$

has to be solved on the macroscale, but a constitutive equation $\bar{\mathbf{q}}$ prescribing the flux over a rough surface is not represented by the classical REYNOLDS flux. Hence an explicit

constitutive equation $\bar{\mathbf{q}}$ is not known. Rather, the *homogenized macroscopic flux* $\bar{\mathbf{q}}$ is extracted from a rough microscale problem that is associated with the macroscale interface at each numerically relevant point, e.g. the integration point. This interface sample problem will be solved as follows:

1. compute macroscale variables from a flat surface macroscale problem, using the mass balance (regarding cavitation in Eq. (2.3) but without substituting the REYNOLDS flux form)
2. where cavitation does not occur, pass macroscale variables to the microscale and incorporate them as boundary conditions on the test sample,
3. solve a rough surface microscale problem, using REYNOLDS equation (Eq. (2.3) neglecting cavitation), for the local flux \mathbf{q} ,
4. compute the macroscale flux $\bar{\mathbf{q}}$ by surface averaging the local flux and pass it to the macroscale,
5. solve the macroscale problem using the macroscale flux $\bar{\mathbf{q}}$, which now transmits the effects of surface roughness to the macroscale.

Steps 2–4 constitute the *micromechanical test*, see Sects. 3.2 and 3.3. To any position in the lubricant at the macroscopic scale such a micromechanical test is attached. Within the finite element framework, this is done naturally at the Gauss points. Unlike the classical homogenization setting for the REYNOLDS equation, however, it is not sufficient to solve these attached problems only once in a pre-processing step. Rather, they must be solved simultaneously throughout the macroscopic deformations steps. This is the typical FE^2 framework for the computational homogenization of heterogeneous media—see earlier cited references.

The validity of the proposed multiscale analysis framework is assessed through the following conditions:

$$\begin{aligned} \bar{\sigma} &= \mathcal{O}(\bar{h}) \ll \bar{c} \\ \sigma &= \mathcal{O}(h) \ll c \\ c &\ll \bar{c} \end{aligned} \quad (3.2)$$

Equations (3.2)_{1,2} ensure that a lubrication formulation holds on the *macroscale* as well as on the *microscale*. Here $\bar{\sigma}$ and σ denote the standard deviations of roughness whereas the representative length of the flowpath is given via \bar{c} and c for the macroscopic and microscopic problems, respectively. Finally, (3.2)₃ is required to justify the separation of scales that is essential for scale-independent homogenization [49, pp. 9–14]. The separation of scales also justifies the split of the micromechanical testing procedure, which is the subject of the next section.

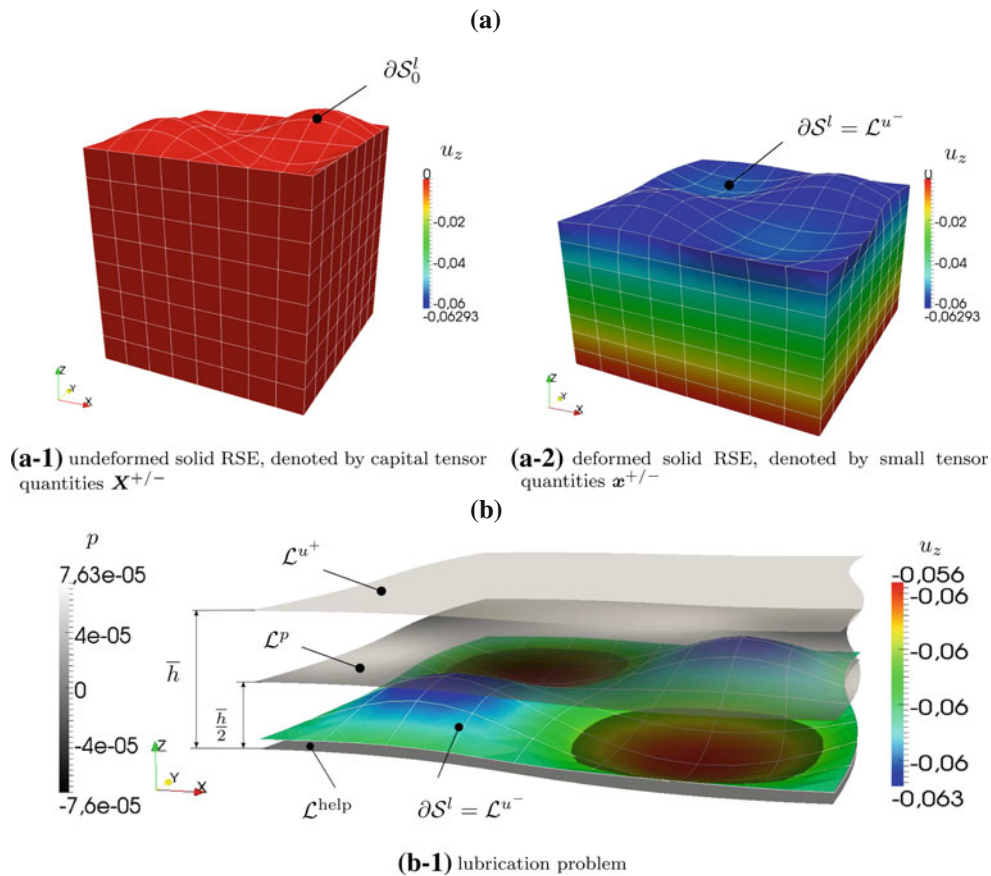


Fig. 5 Micromechanical split: (a) mechanical phase, subject to $\mathbf{x}^+ - \mathbf{x}^- = \bar{\mathbf{F}}^S (\mathbf{X}^+ - \mathbf{X}^-)$ and (b) lubrication phase, subject to $p^+ - p^- = \hat{\mathbf{g}} \cdot (\mathbf{X}^+ - \mathbf{X}^-)$

3.2 Two-phase micromechanical test

The introduced *micromechanical test* can be split into a (i) *mechanical phase* followed by a (ii) *lubrication phase* and through which an efficient numerical treatment of the homogenization problem can be achieved. This procedure is visualised in Fig. 5 and flowchart Fig. 7, however important information on setting up the procedure is contained in this section. The split is exact to within a separation of scales assumption [55, Sect. 3]. If not employed, the solution of the coupled problem, which is now numerically more expensive, would additionally require an explicit satisfaction of (3.2)₃ by choosing the sample small in terms of absolute length scale. When not appropriately chosen, the sample size can influence the macroscopic flux for a given set of boundary conditions. However, such a sample size dependence is not allowed when a separation of scales is admitted. Consequently, the split of the testing procedure ensures an automatic satisfaction of this condition.

Within the mechanical phase a purely mechanical problem undergoing finite deformations will be solved. The deformation is induced by:

- the macroscopic fluid pressure ($\bar{p} \approx const$) acting as a follower load (subject to being linearised) on the top surface S_0^l of the *Representative Surface Element (RSE)*,
- the macroscale deformation $\bar{\mathbf{F}}^S = \mathbf{1} + \bar{\mathbf{H}}^S$ (applied to the side surfaces $\partial S^{+/-}$ of the RSE; see Sect. 3.3 and Fig. 6 and Stupkiewicz [49], Temizer and Wriggers [54]), and
- the chosen geometry (roughness) of top surface ∂S_0^l .

Outcome is a deformed surface \mathcal{L}^{u^-} . Employing a constant pressure within the mechanical phase agrees with the asymptotic expansion analysis of Bayada et al. [8] and is consistent with the separation of scales.

Subsequently, the *lubrication phase* can be constructed using the deformed surface \mathcal{L}^{u^-} , see Fig. 5b. In order to form a thin channel, a flat surface \mathcal{L}^{u^+} is placed at a distance \bar{h} above the mean plane of the rough surface \mathcal{L}^{u^-} . For this purpose, introducing

$$\langle \bullet \rangle = \frac{1}{A_0} \int_{\mathcal{L}^{u^-}} \bullet \, da \quad \longrightarrow \quad \bar{h} = \langle h \rangle, \quad \bar{z} = \langle z \rangle, \quad (3.3)$$

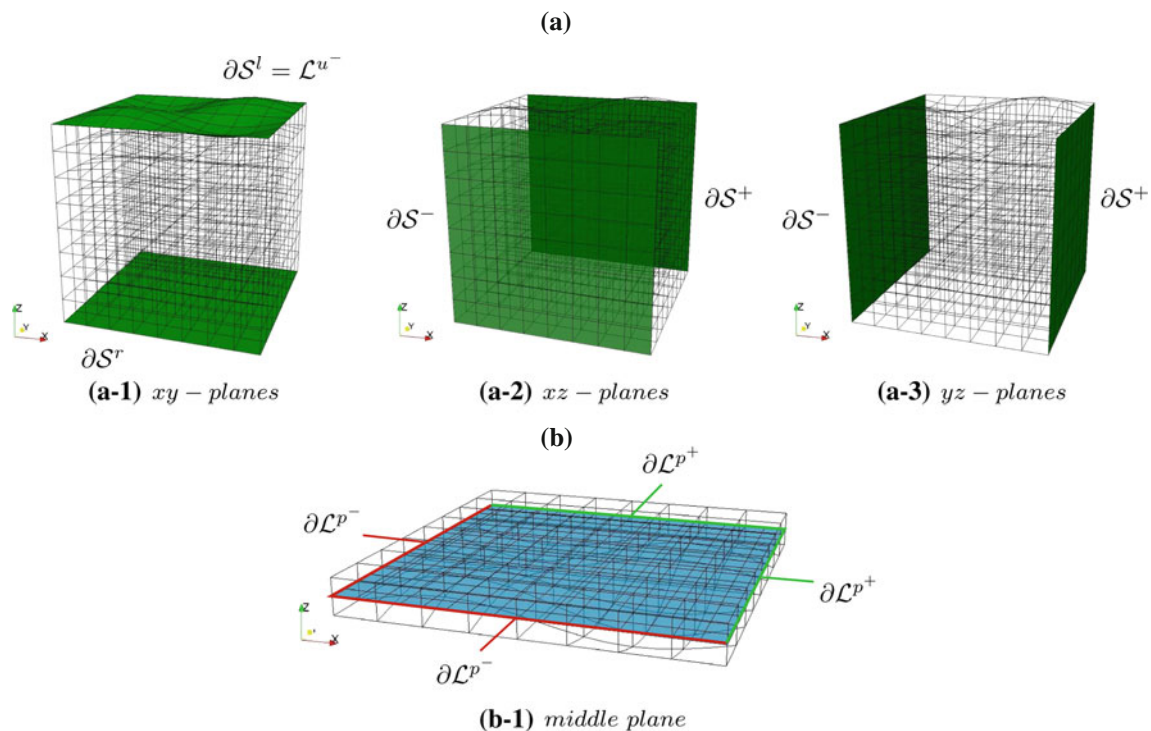


Fig. 6 Notation of boundaries on (a) the mechanical phase and (b) the lubrication phase

at position \bar{z} a flat surface \mathcal{L}^{help} is placed with respect to which the top surface \mathcal{L}^{u+} is at an average distance \bar{h} with respect to the rough surface \mathcal{L}^{u-} .

Due to computational reasons (Sect. 2.2) an intermediate surface \mathcal{L}^p is introduced to compute and store the lubricant local pressure p . The lubrication problem is subject to the following restrictions:

- the top surface is forced to be under tangential motion \bar{v} but \mathcal{L}^{u-} is fixed and
- the macroscopic pressure gradient \bar{g} acts on \mathcal{L}^i , refer to Sect. 3.3 and Fig. 6.

The former assumption is particularly convenient because it allows a static analysis and is a common starting point in many works [1, 2, 4, 8, 10, 12, 18, 25, 26, 41]. In contrast to this setting, two rough surfaces moving against another or accounting for tangential contact demands a time dependent analysis [30, 33, 35, 50, 57].

Since the pressure distribution is not constant throughout the microscale for a rough surface, q is of “fast varying” character. Hence it must be averaged before passing it to the macroscale:

$$\bar{q} = \langle q \rangle \quad (3.4)$$

3.3 Boundary conditions

At each Gauss point the global variables $(\bar{h}, \bar{p}, \bar{g}, \bar{v}, \bar{F}^S, \text{geometry})$ are passed to the micromechanical test proce-

dure, where they are incorporated as boundary conditions. They satisfy the following aspects:

- the exact homogenized response is delivered from a unit-cell analysis if the microstructure is periodic [53] (Fig. 9 and
- the macroscopic quantities that appear in the boundary conditions are recovered by surface averaging [53] (Sect. 3.2, in particular $\bar{g} = \langle g \rangle$).

In the *mechanical phase*, at the bottom layer ∂S_0^l all nodal movements are restricted in the z-direction. Additionally one of these nodes $x \in \partial S_0^l \setminus \partial S_0^i$ has to be fixed in all directions to avoid rigid body motions. On the side surfaces ∂S_0^i periodic boundary conditions are imposed to transfer global deformations to the *microscale* (see Eq. (3.5) and Fig. 6a). On the rough surface ∂S_0^l traction boundary conditions are applied as a non-conservative loading, cf. Eq. (3.6).

$$x^+ - x^- = \bar{F}^S (X^+ - X^-), \text{ on } \partial S^i = \partial S^- \cup \partial S^+ \quad (3.5)$$

$$t = -\bar{p}n, \quad \text{on } \partial S^l \quad (3.6)$$

Within the *lubrication phase* periodic boundary conditions are used to obtain the pressure distribution on the middle plane nodes. Therefore the side nodes of the middle plane are restricted as follows:

$$p^+ - p^- = \bar{g} \cdot (X^+ - X^-), \text{ on } \partial \mathcal{L}^i = \partial \mathcal{L}^{p-} \cup \partial \mathcal{L}^{p+} \quad (3.7)$$

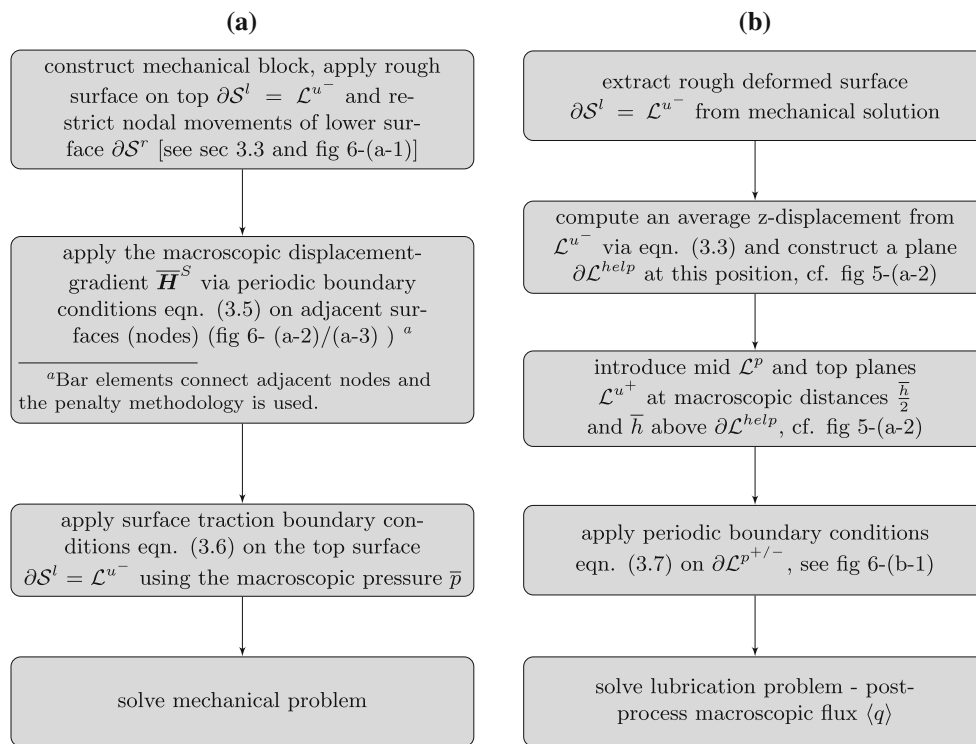


Fig. 7 The Flowchart for the two-phase micromechanical test, see Sect. 3.2 (a) Mechanical phase (b) the Lubrication phase

A single node on $\delta\mathcal{L} \setminus \partial\mathcal{L}^i$ is restricted to zero pressure and all nodes are restricted to zero displacement, see Fig. 6b. Beforehand the lubrication channel is constructed by making use of \bar{h} , see Figs. 5b and 7b. The tangential relative motion \bar{v} between the upper and lower surfaces directly goes into Eq. (2.1).

Analogous to Eq. (3.1), \bar{q} satisfies $-\rho \operatorname{div}[\bar{q}] = 0$. In case when there is a normal relative velocity between the surfaces it is necessary to modify the macroscopic mass balance (Eq. 3.1) by introducing appropriate rate of normal separation on the right hand side, see [22,51]. However no modification is needed on the microscale: $-\rho \operatorname{div}[\mathbf{q}] = 0$ still holds. The omission of such dynamic terms from the microscale problem is standard, e.g. in elastodynamics the computation of the effective elastic constants does not require the consideration of acceleration on the microscale, see [61]. These results are supported by asymptotic expansion approaches in homogenization, see earlier cited references.

3.4 Identification of macroscopic quantities

From Sect. 3.2 it is known that surface averaging microscopic local quantities gives us macroscopic values and hence the macroscopic flux is identified as $\bar{q} = \langle \mathbf{q} \rangle$. To study whether a macroscopic constitutive equation can be identified the flux \bar{q} is decomposed additively for observation purposes as is used in Sect. 4

$$\bar{q} = \bar{q}^p + \bar{q}^c, \quad \begin{cases} \bar{q}^p = \langle \mathbf{q}^p(h, p, \mathbf{g}) \rangle \\ \bar{q}^c = \langle \mathbf{q}^c(h, \bar{v}) \rangle \end{cases} \quad (3.8)$$

To identify macroscopic quantities $(\bar{h}, \bar{p}, \bar{\mu}, \bar{\mathbf{g}})$ via surface averaging to obtain a macroscopic constitutive equation, one proceeds by

$$\begin{aligned} \langle \mathbf{q} \rangle &= \left\langle -\frac{h^3}{12\bar{\mu}} \mathbf{g} + \frac{h\bar{v}}{2} \right\rangle, \quad \begin{cases} \bar{\mu} = \mu(\bar{p}) \\ \mathbf{g} = \operatorname{grad}(p) \end{cases} \\ &= -\frac{1}{12\bar{\mu}} \langle h^3 \mathbf{g} \rangle + \frac{\bar{v}}{2} \underbrace{\langle h \rangle}_{\equiv \bar{h}} \\ &= -\frac{1}{12\bar{\mu}} \langle h^3 \mathbf{g} \rangle + \frac{\bar{h}\bar{v}}{2} \\ &= \bar{q}^p + \bar{q}^c(\bar{h}, \bar{v}) \end{aligned} \quad (3.9)$$

and hence a classical COUETTE term is obtained but the Poiseuille term cannot be expressed as a function of macroscopic quantities explicitly. It is this term that makes an explicit homogenization analysis necessary, even when the rough surface is rigid.

3.5 A micro–macro dissipation equality

In a full Navier–Stokes representation of the fluid, dissipation is induced by the viscous flow which causes temperature rise in the fluid. A consideration of the dissipation effects has been carried out by Cope [14] by simplifying the energy equa-

tion under the Reynolds equation assumptions that lead to the thin-film limit. The results obtained have subsequently been verified by Charnes et al. [13] through an alternative deri-

vation where the energy-dissipation relationship was characterized under the thin-film assumptions. Now, since no energy is stored by an incompressible fluid under steady state

Table 2 Material parameters employed in Sect. 4 are summarized

Solid (Neo Hook)			
Young’s modulus (N/mm ²)	E	475.0	
Poisson’s ratio	ν	(0.0–[0.499])	Sect. 4.1
Block dimensions (mm)	$l_x \times l_y \times l_z$	$0.2 \times 0.2 \times 0.4$	
Roughness amplitude (mm)	\widehat{z}	0.01	
Number of quadratic elements	x,y,z	$8 \times 8 \times 16$	
Fluid pressure (MPa)	\bar{p}	(0.0–[5.0])	Sect. 4.1
Surface geometry		iso-/ anisotropic	Sect. 4.2
Displacement gradient	\overline{H}^S	(-1.0,[0.0],1.0)	Sect. 4.3
Lubricant (Water)			
Velocity (mm/s)	\bar{v}_β	2356.0 ($\bar{g} = 0$)	
Pressure gradient (MPa/mm)	\bar{g}_β	0.1 ($\bar{v} = 0$)	
Angle of orientation w.r.t. x-axis (MPa/mm)	β	[0.0]–360.0	
Gapheight (mm)	\bar{h}	([0.05]–0.1)	Sect. 4.2
Viscosity (at 20 °C) (MPa s)	μ	$1.0 \cdot 10^{-9}$	
Pressure–viscosity coefficient (Pa ⁻¹)	α	0.0	
Number of quadratic elements	x,y,z	$8 \times 8 \times 1$	

Unless otherwise noted the values in brackets [•] are used

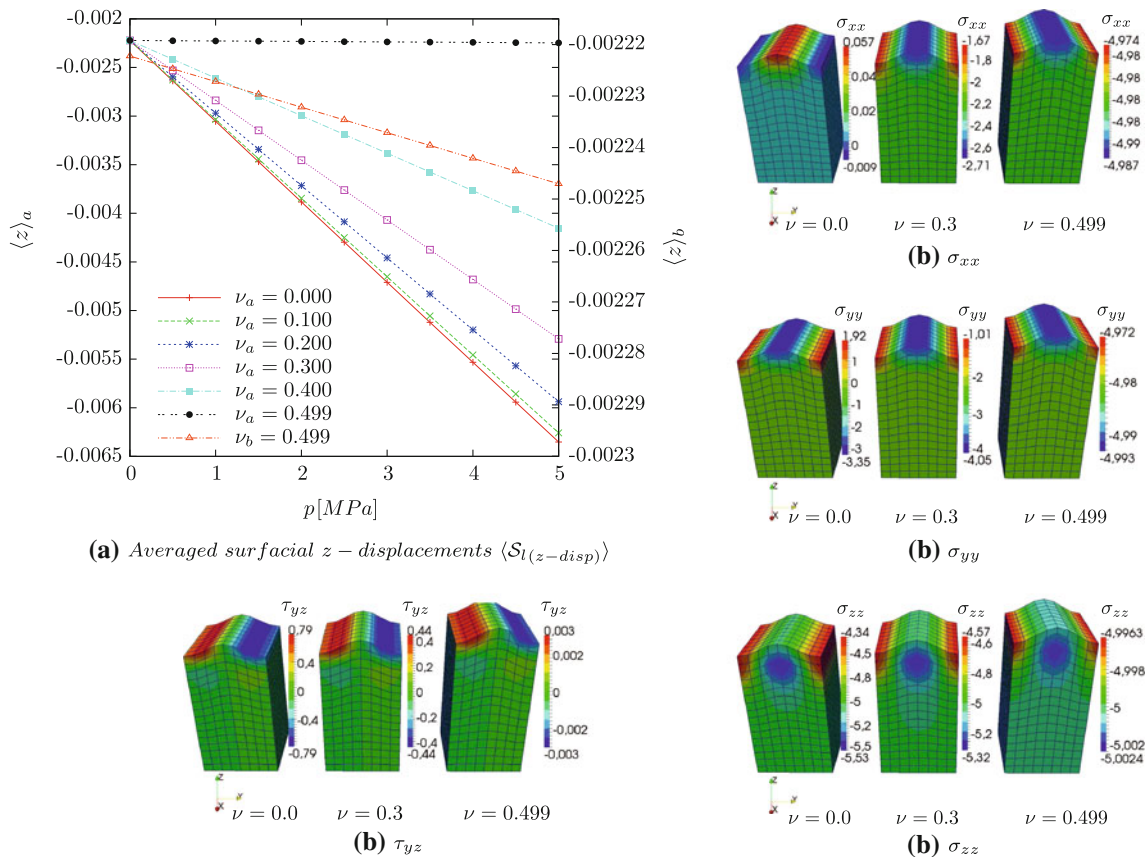


Fig. 8 Influence of Poisson’s ratio ν on: (a) surfacial z -displacements when an increasing pressure load p (Poisson’s ratio $\nu = 0.499$ is additionally plotted w.r.t. a different range to highlight small changes in the geometry) and (b) stress distribution to be subject of $\bar{p} = 5$ MPa

conditions, the local dissipation \mathcal{D} on the microscale must match the power input \mathcal{P} . Therefore, in order to preserve dissipation through the scale transition of homogenization, the following equivalent conditions must be satisfied:

$$\overline{\mathcal{D}} = \langle \mathcal{D} \rangle \iff \overline{\mathcal{P}} = \langle \mathcal{P} \rangle. \tag{3.10}$$

In this work, the effect of the shear stresses are omitted. Consequently, the power input is expressed only in terms of the flow work \mathcal{P}_f [13]:

$$\mathcal{P} \equiv \mathcal{P}_f = -\mathbf{q} \cdot \mathbf{g}. \tag{3.11}$$

The expression of the flow work is admitted to be of the same form on the macroscale:

$$\overline{\mathcal{P}} \equiv \overline{\mathcal{P}}_f = -\overline{\mathbf{q}} \cdot \overline{\mathbf{g}}. \tag{3.12}$$

Consequently, making use of the macroscopic identifications for the flux (Sect. 3.2) and the pressure gradient (Sect. 3.3), preservation of dissipation across the scales requires satisfying

$$\overline{\mathcal{D}} = \langle \mathcal{D} \rangle \iff -\langle \mathbf{q} \rangle \cdot \langle \mathbf{g} \rangle = -\langle \mathbf{q} \cdot \mathbf{g} \rangle, \tag{3.13}$$

which will be referred to as the *micro–macro dissipation equality*. The satisfaction of this equality is guaranteed by the periodic boundary conditions employed in this work [55] and therefore the thermodynamical consistency of the computational homogenization approach is guaranteed. It is noted that a complete consideration of the dissipation effects requires incorporating shear stress effects as well. However, this requires imposing shear stresses on the rough surface within the mechanical phase of the micromechanical test, the study of which is planned as a future work.

4 Numerical investigations

In this section, major aspects of the proposed computational homogenization framework are highlighted. In Sect. 4.1, primarily the influence of the Poissons ratio ν and surface load \overline{p} is studied at the mechanical phase. Further investigations refer to the lubricant response on changing macroscopic control parameters. For subsequent computations $\overline{\mathbf{g}}$, $\overline{\mathbf{v}}$ have been applied with constant magnitude but changing orientation. Two different surface *geometries* are reviewed in Sect. 4.2 finding isotropic and anisotropic flux behaviours where the importance of the gap height \overline{h} is additionally demonstrated. The effect of the displacement gradient $\overline{\mathbf{H}}^S$ will be highlighted in Sect. 4.3. In all other investigations $\overline{\mathbf{H}}^S$ will be set to zero. see Table 2 for the default simulation parameters employed.

4.1 Effects of solid incompressibility

To investigate the influence of an incompressible solid onto the surface deformation, a computational test was carried out on six specimens with varying Poisson’s ratio ν (Fig. 8). The specimens have been loaded with increasing pressures \overline{p} acting normal to the top surface ∂S_0^l of each block, such that the viewer observes decreasing displacement of the top surfaces as well decreasing stress variations from low to high Poisson’s ratio $\nu = 0.0 \rightarrow 0.499$ (Fig. 8a,b). The degree of variation in the asperity stress is observed to heavily depend on ν .

Two important observations can be made regarding these results. First, for incompressible hyperelastic materials, the effect of the pressure on asperity deformation is negligible. Consequently, the lubrication phase, which is governed primarily by the surface microstructure, will not be influenced significantly by the pressure within the micromechanical testing procedure. However, on the macroscale the pressure may induce surfacial stretches $\overline{\mathbf{H}}^S$, in particular near free edges, which will be observed to have a significant effect on the lubrication response (Sect. 4.3). Similarly, for compressible materials, it has been verified that although large sample compressions are observed, the statistical characteristics of the surface do not vary significantly in the range of pressures investigated (not shown). On the other hand, such large compressions are important because these change the gap height on the macroscopic interface and consequently

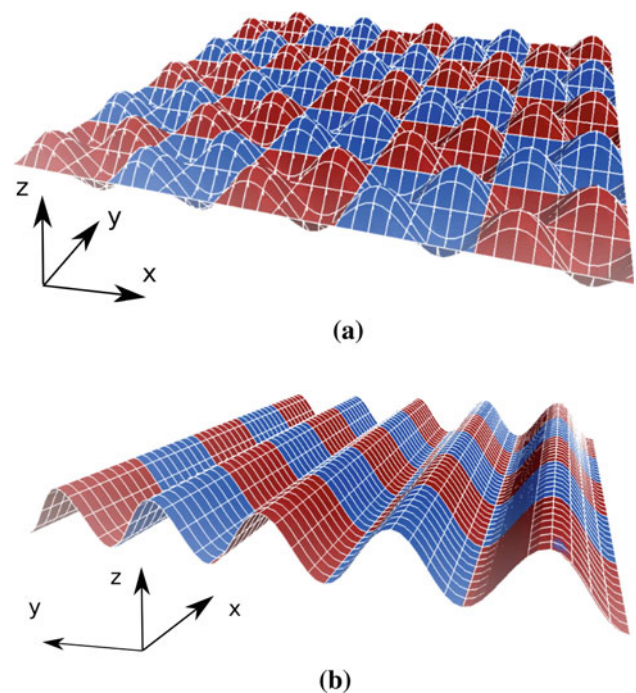
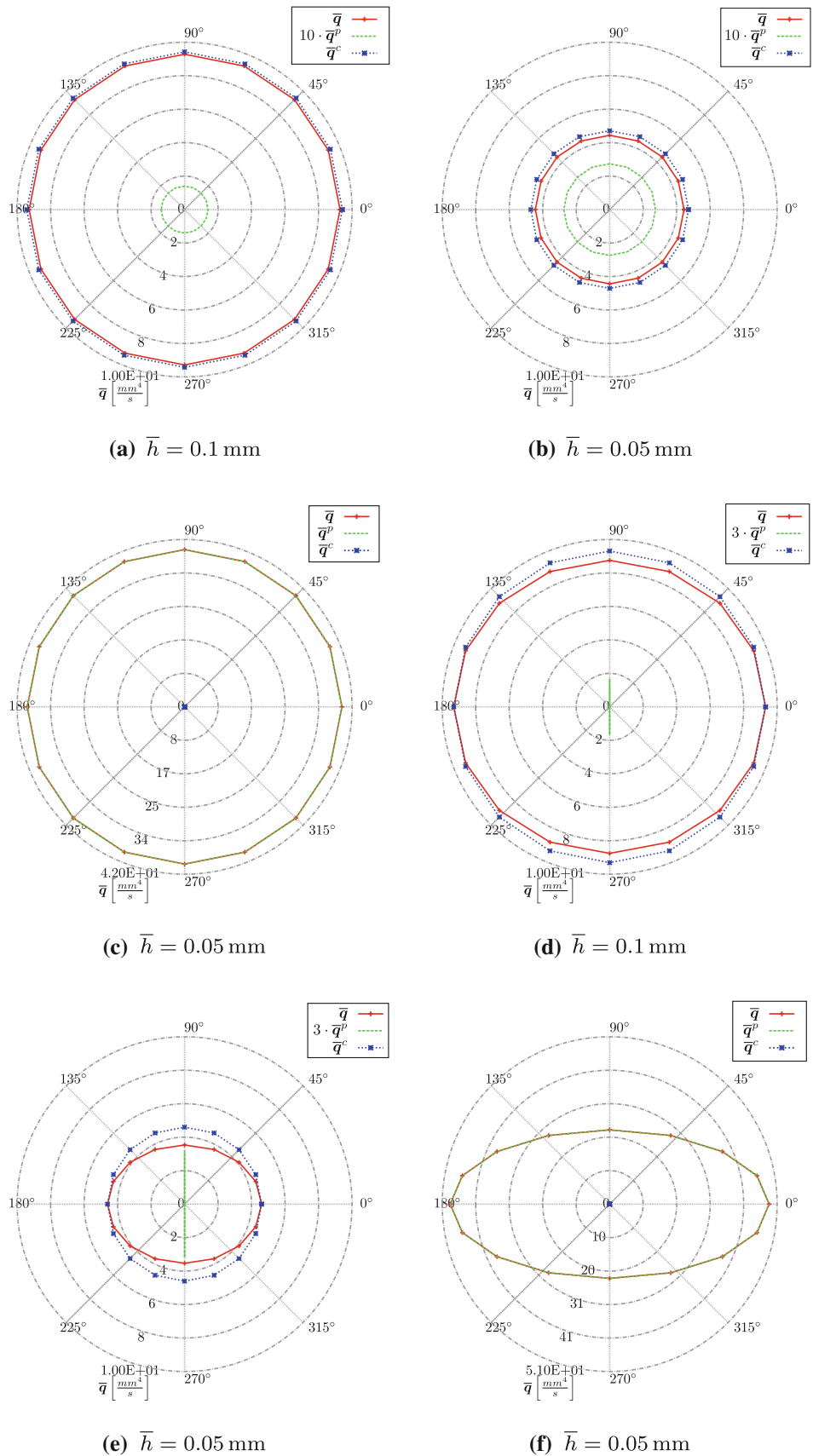


Fig. 9 Isotropic and anisotropic surface. Amplitudes are scaled by a factor of five: (a) isotropic (b) anisotropic

Fig. 10 Influence of decreasing gap height \bar{h} on global flux orientation and magnitude on (a, b, c) *isotropic* surface and (d, e, f) *anisotropic* surface. For subfigure (c,f) $\bar{v} = 0$ mm/s and $\bar{g} = 0.1$ MPa/mm were applied. All other results have been computed using $\bar{v} = 2356$ mm/s and $\bar{g} = 0$ MPa/mm



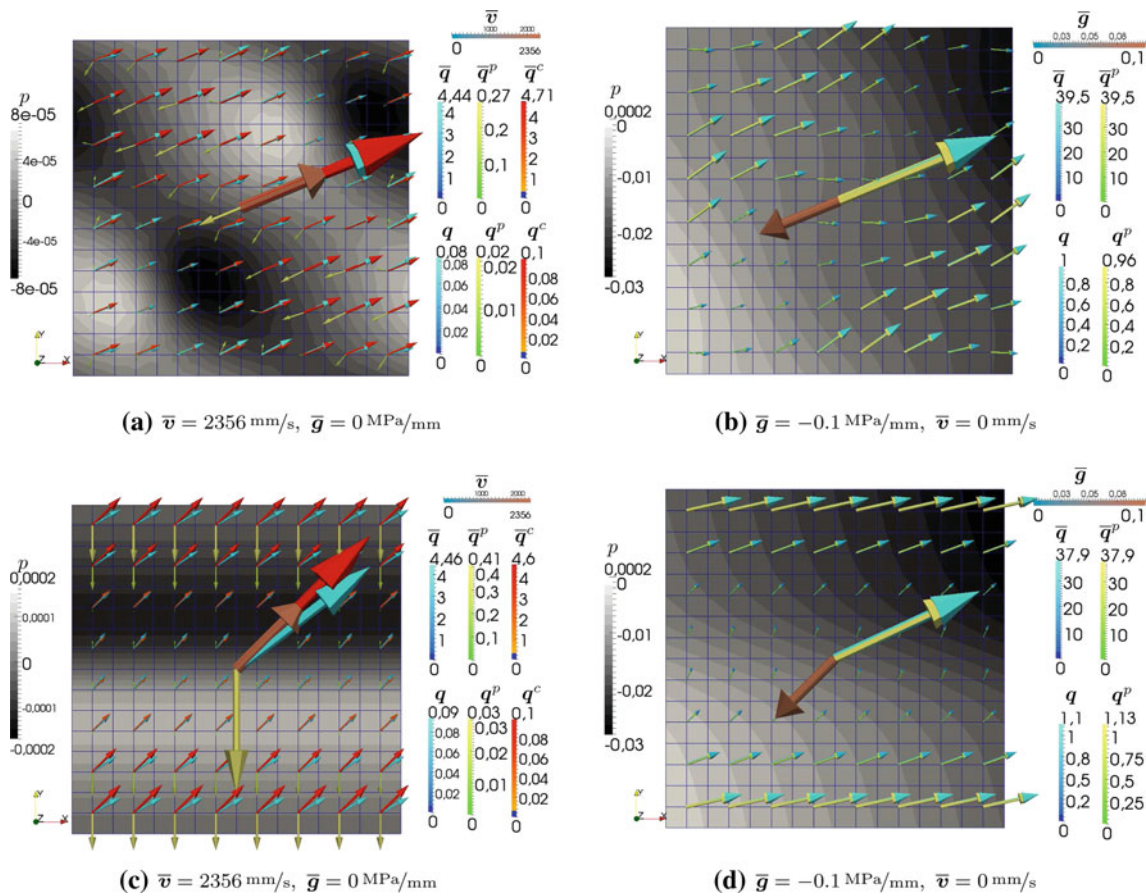


Fig. 11 Computational results of local flux, pressure distribution (q, q^p, q^c, p) and total flux ($\bar{q}, \bar{q}^p, \bar{q}^c$) on (a, b) isotropic surface and (c, d) anisotropic surface, q.v. Fig. 9. Both input parameters \bar{v} and \bar{g} are applied to (a, b) at an angle of $\beta = 22.5^\circ$ and to (c, d) at an angle of $\beta = 45^\circ$ with respect to x-axis. The surface color shows the local pressure distribution p in the lubricant flow. High pressures are

coloured white and low pressures are coloured black. Arrows represent the magnitude and orientation of input parameters \bar{v}, \bar{g} and output variables q, \bar{q} and its components. They are clearly allocated by the legend. The input and macroscopic output quantities, and hence their corresponding arrows are centered. Local fluxes are centered on their corresponding elements

alter the flow characteristics in the macroscopic elastohydrodynamic lubrication problem, cf. Szeri [51, p. 410]. A fully coupled micro–macro simulation strategy where the coupling between microscopic and macroscopic mechanisms can be clearly observed is planned for a future work.

4.2 Anisotropic/isotropic surfaces

Computing the global flux \bar{q} can deliver information on whether macroscopically isotropic or anisotropic flow conditions are present and hence whether the surface is deemed isotropic or anisotropic for the purposes of lubrication characterization. Isotropy exists when the input parameter \bar{v}_β or \bar{g}_β , only one of them being active for arbitrary angles β (angle between the x-axis and flow direction, compare with Fig. 11), cause a flux \bar{q}_β such that

$$\begin{aligned}
 (\bar{v}_\beta \text{ or } \bar{g}_\beta) \parallel \bar{q}, \quad \text{and} \quad \|\bar{q}\| = \text{const} \quad \forall \beta \\
 \Rightarrow S_0^I \text{ isotropic}
 \end{aligned}
 \tag{4.1}$$

holds. Anisotropy is characterized by

$$\begin{aligned}
 \exists \beta \quad (\bar{v}_\beta \text{ or } \bar{g}_\beta) \not\parallel \bar{q}, \quad \text{or} \quad \|\bar{q}\| \neq \text{const} \quad \forall \beta \\
 \Rightarrow S_0^I \text{ anisotropic}
 \end{aligned}
 \tag{4.2}$$

Therefore parameter studies with changing orientation of \bar{v}_β and \bar{g}_β have been carried out on two different surfaces (Fig. 9), where $\beta \in 0^\circ\text{--}360^\circ$ was incremented in steps of 7.5° .

Figure 10 illustrates the macroscopic flux response \bar{q} for these studies. Here figures (a,b,d,e) in the first and second column are subject to macroscopic velocity \bar{v}_β and figures (c,f) in the third column are subject to the macroscopic pressure gradient \bar{g}_β . The isotropic surface (Fig. 9a) was applied to figures (a,b,c) in the first row whereas figures (d,e,f) in the second row are subject to the anisotropic surface (Fig. 9b). Each cross in the plots relates the flux \bar{q} and its components to an input parameter \bar{v} or \bar{g} . For the start angle of $\beta = 0^\circ$

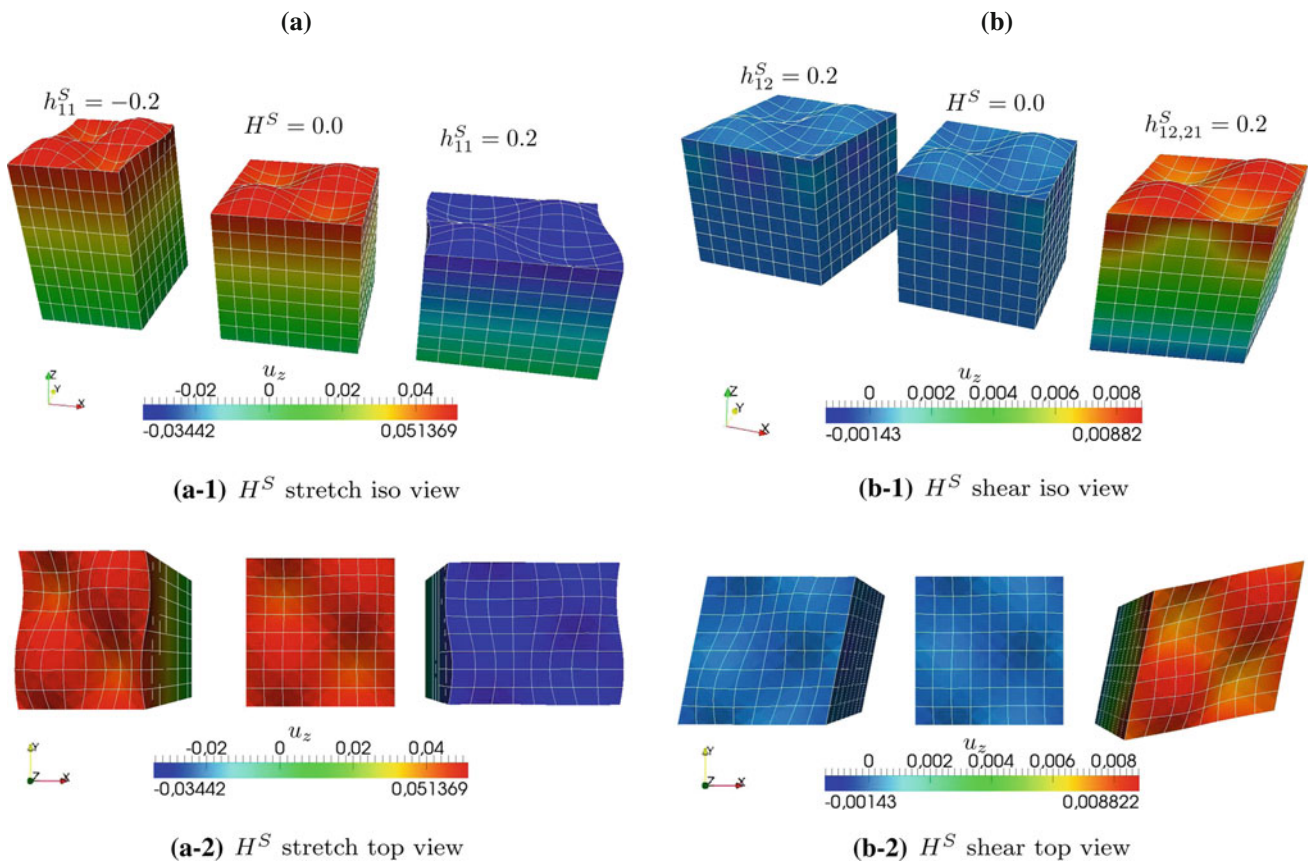


Fig. 12 Mechanical phase undergoing (a) a stretch into h_{11}^S direction and (b) a shear into $h_{12,21}^S$ direction and being subject to periodic boundary conditions

the computed fluxes are in phase with \bar{v} (Fig. 10a, b, d, e), but phase-shifted by 180° for \bar{g} (Fig. 10c, f). Moving inside a plot in counterclockwise direction with increments of 7.5° one observes a circular flux response \bar{q} and uniformly distributed crosses in Fig. 10a–c meaning that Eq. (4.1) is fulfilled, hence the surface is isotropic. Note that for isotropy the flux components \bar{q}^p and \bar{q}^c display the same characteristics as \bar{q} . Reviewing Fig. 10d–f an anisotropic response is observed via Eq. (4.2). Here, the flux \bar{q} has an elliptic form. Among its components, \bar{q}^p is directed along the vertical direction (but with varying magnitude) whereas \bar{q}^c remains isotropic (circular). For Fig. 10f the COUETTE term \bar{q}^c vanishes such that $\bar{q} = \bar{q}^p$ causes anisotropy. Reducing the gap height \bar{h} restricts the flow and hence leads to a decrease in the flux magnitude for both isotropic and anisotropic surfaces, compare Fig. 10a, b, d, e. Furthermore, an increase of ellipticity and hence anisotropy for an anisotropic geometry can be observed comparing Fig. 10d, e.

A discussion of the macroscopic flux components \bar{q}^p and \bar{q}^c requires monitoring their microscopic counterparts q^p and q^c . Figures 11a, c illustrate that the orientation of the

COUETTE flow on both scales (i.e. \bar{q}^c and q^c) remain parallel to the input velocity \bar{v} at all times. Hence the COUETTE term always causes an isotropic flux, which is clear from its constitutive form. The local flux q^c changes proportionally to the local gap height h (Eq. 4.3) which can be identified in Eq. (2.2), whereas its macroscopic equivalent remains constant for all angles β .

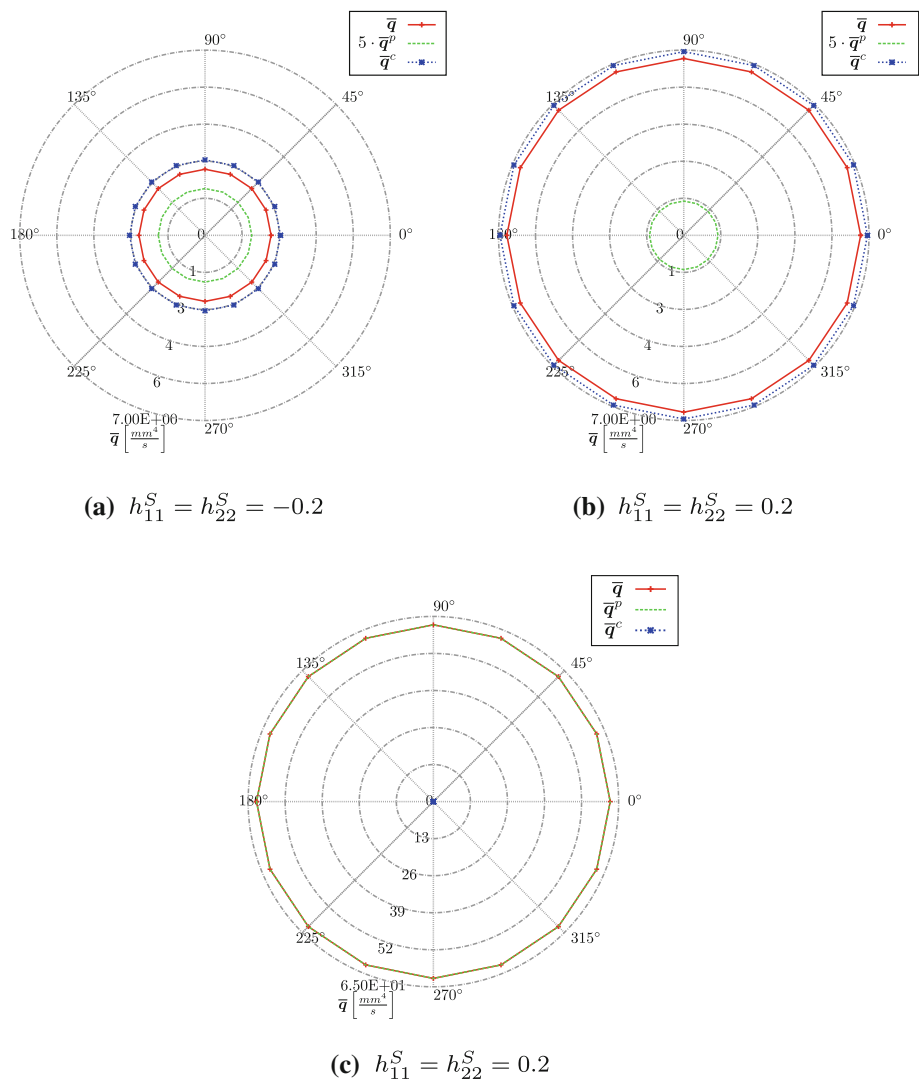
$$\|q^c\| \propto h, \text{ if } \bar{v} = \text{const} \tag{4.3}$$

Due to the fact that $\bar{v} = 0$ mm/s for plots in Fig. 11b, d the COUETTE term vanishes ($q^c = \bar{q}^c = 0$) such that

$$\begin{aligned} q &= q^p \text{ and } q^c = 0, \text{ for } \bar{g} \neq 0 \text{ and } \bar{v} = 0 \text{ and} \\ \bar{q} &= \bar{q}^p \text{ and } \bar{q}^c = 0, \text{ for } \bar{g} \neq 0 \text{ and } \bar{v} = 0, \end{aligned} \tag{4.4}$$

hold. Flow deflection is caused by the POISEUILLE terms \bar{q}^p and q^p depending on the pressure gradient \bar{g} as well the gap height h and thus the surface microstructure. Arrows representing the Poiseuille fluxes q^p and \bar{q}^p also help visualize pressure gradients. They always point from high pressure areas towards low pressure areas (Fig. 11).

Fig. 13 Isotropic response of an isotropic surface undergoing uniform stretch into h_{11}^S and h_{22}^S direction: **(a, b)** $\bar{v} = 2356$ mm/s, $\bar{g} = 0$ MPa/mm and **(c)** $\bar{g} = 0.1$ MPa/mm, $\bar{v} = 0$ mm/s



4.3 Deformation gradient

The influence of the surfacial deformation gradient is investigated in this section. In matrix notation,

$$\bar{\mathbf{F}}^S = 1 + \bar{\mathbf{H}}^S, [\bar{\mathbf{H}}^S] = \begin{bmatrix} h_{11}^S & h_{12}^S \\ h_{21}^S & h_{22}^S \end{bmatrix} \quad (4.5)$$

where the entries on the main diagonal h_{ii}^S stretch a surface, and hence the remaining entries $h_{ij}^S, i \neq j$ shear a surface, cf. Fig. 12.

For $h_{11}^S = h_{22}^S = (-0.2 \rightarrow 0.2)$ isotropy is preserved for velocity and pressure gradient driven computations (see Fig. 13). As a consequence of surfacial stretch roughness is flattened, and hence flux increases.

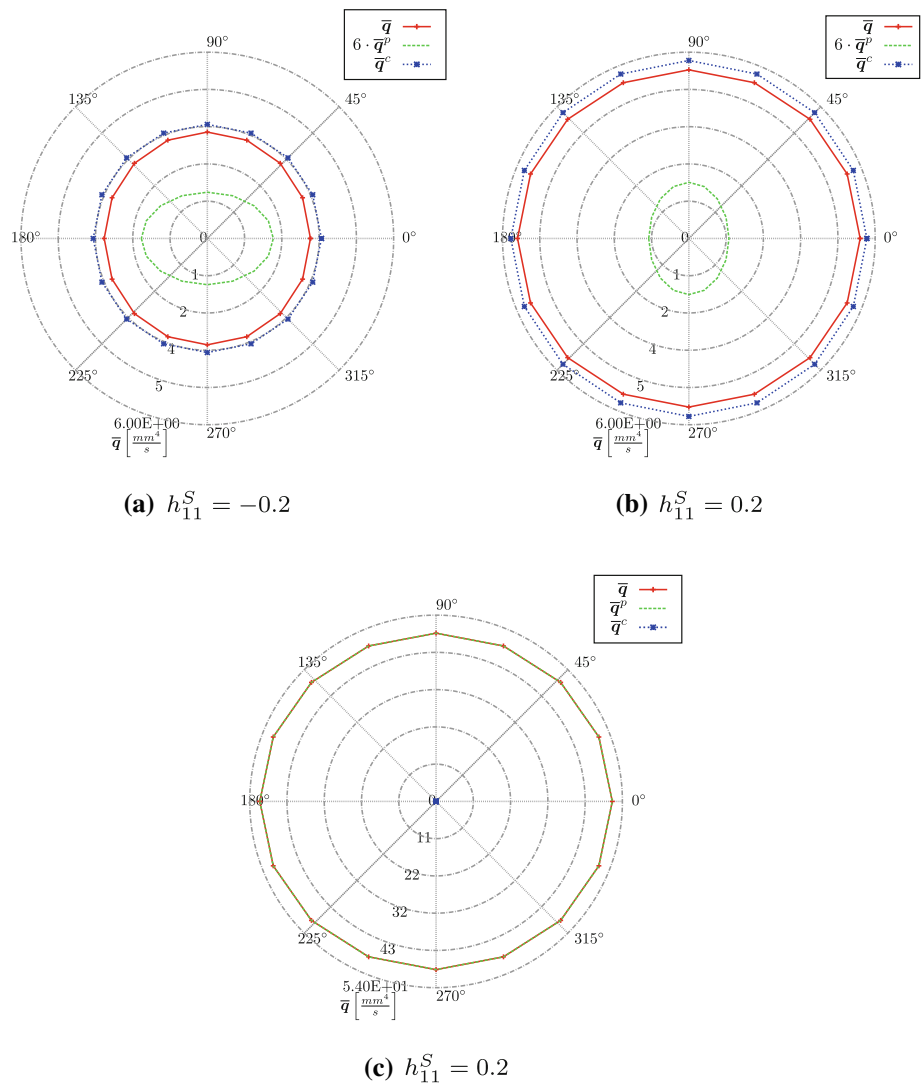
Solely varying the displacement component $h_{11}^S = (-0.2 \rightarrow 0.2)$ gives an anisotropic response. It can be observed for $h_{11}^S = -0.2$ in Fig. 14a that \bar{q}^p has an elliptical shape. Its principal direction points towards 0° and causes

an elliptical flux \bar{q} with principal direction pointing towards 90° . Applying a positive displacement gradient $h_{11}^S = 0.2$ (Fig. 14b) orientation of both fluxes (\bar{q}^p, \bar{q}) turns about 90° . Additionally, an increase of flux from negative to positive displacement gradients can be seen due to an increasing surface.

For a pressure gradient $\bar{g} = 0.1$ MPa/mm driven computation (Fig. 14c) the flux \bar{q} keeps its principal directions towards 0° ($h_{11}^S = 0.2$) and hence it follows \bar{q}^p according to our observations in Sect. 4.2.

Finally, the effect of the shearing components are evaluated. This effect is not as dominant compared to stretching. Therefore, the values have been chosen larger, but remaining in a realistic deformation range, to show its influence on the anisotropic behaviour. Varying $h_{12}^S = 0.3 \rightarrow 0.9$ causes an increasing anisotropic flux response (Fig. 15a–c). Further on the COUETTE flux q^c principal direction moves from $\approx 30^\circ$ towards $\approx -30^\circ$ and hence the flux \bar{q} is shifted by 90° .

Fig. 14 Anisotropic response of an isotropic surface stretched along the 0° axis: **(a, b)** $\bar{v} = 2356 \text{ mm/s}$, $\bar{g} = 0 \text{ MPa/mm}$ and **(c)** $\bar{g} = 0.1 \text{ MPa/mm}$, $\bar{v} = 0 \text{ mm/s}$. Only the POISEUILLE term \bar{q}^p contributes to the total flux \bar{q} and hence they coincide



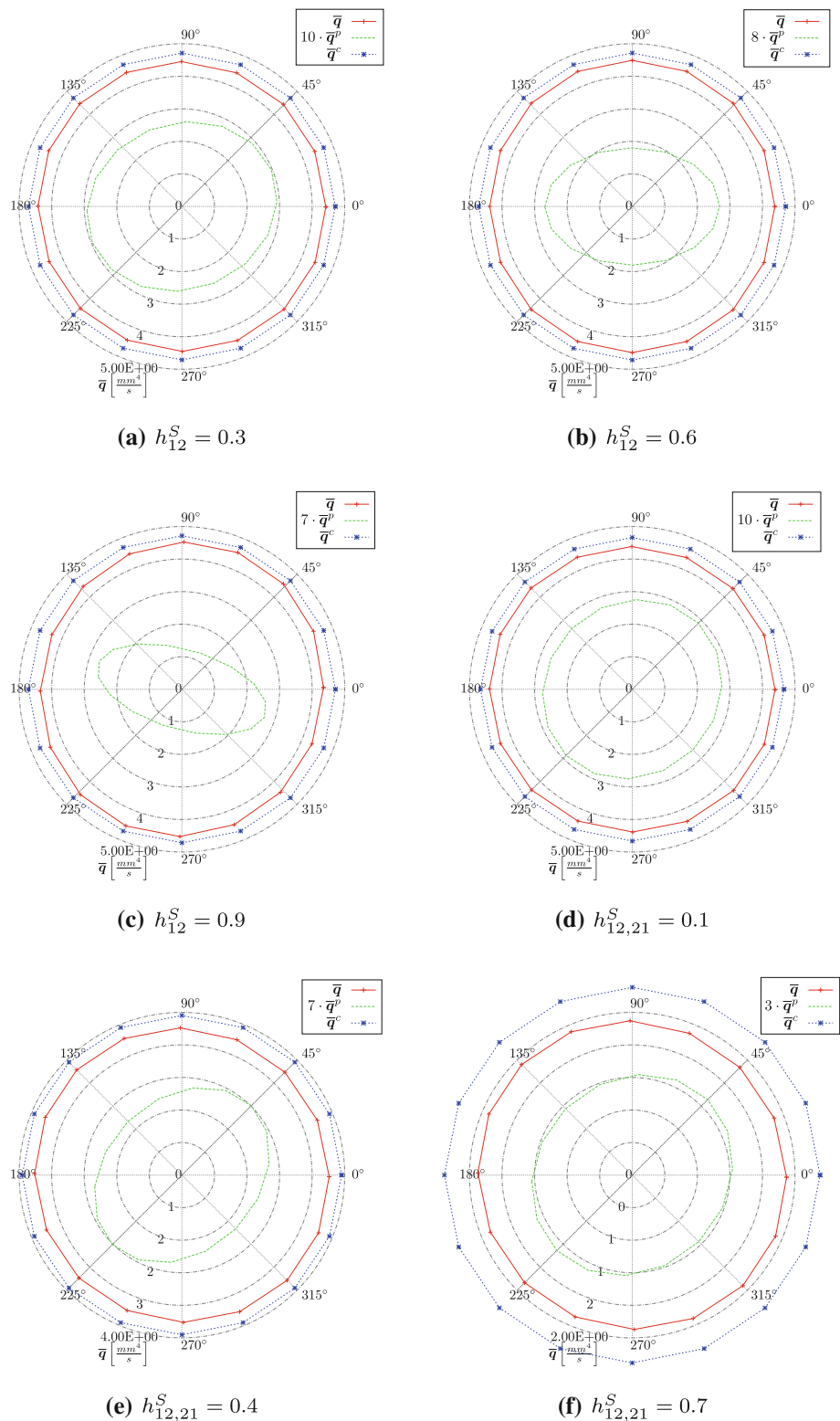
Applying $h_{12}^S = h_{21}^S = 0.1 \rightarrow 0.7$ causes a stronger surface shrinking and also a strong elliptical response (Fig. 15d–f). The principal direction of the flux \bar{q} points towards 45° . Pressure gradient \bar{g} induced fluxes are summarized in Fig. 16. Here, another data representation was chosen to elucidate shearing influence. Again a shrinking surface can be observed for solely varied parameters $h_{i,j}^S$, $i, j \in 1, 2 \wedge i \neq j$ as well as a moderate anisotropy. A stronger response is observed for shearing $h_{12}^S = h_{21}^S$ at the same time.

5 Conclusion

Solving a macroscale lubrication problem making use of REYNOLDS equation while taking into account surficial microscopic roughness that is several orders of length scales smaller demands a very fine mesh resolution and hence prohibitive computational times. In order to predict

the macroscopic response of microscopically rough lubricated interfaces in the large deformation regime within feasible computational times, a three-dimensional computational homogenization approach was presented, closely following homogenization techniques for rigid and infinitesimally deforming surfaces. The approach is based on proposing a lubrication formulation governed by the classical REYNOLDS equation on the microscale, in agreement with earlier approaches, but extracting the macroscopic flux within a micromechanical testing procedure. While the problem remains coupled on the macroscale, the macroscopic flow control parameters are projected onto the micromechanical test sample as boundary conditions such that a *two-phase micromechanical test* was induced. Herein, an effective numerical treatment of a *mechanical phase* followed by a *lubrication phase* is achieved. This two-phase split is exact to within a separation of scales assumption, as in multiphysics homogenization strategies for heterogeneous media. The

Fig. 15 Anisotropic flow behavior for surfacial shearing with $\bar{v} = 2356 \text{ mm/s}$, $\bar{g} = 0 \text{ MPa/mm}$



numerical results presented show that within the interface the fluid flow is strongly influenced by the surface geometry which was found to be significantly altered by the surfacial deformation. The surfacial deformation, in turn, is significantly influenced on the macroscale by the gap height and

the pressure. Qualitative observations could be made for these parameters and have been found to be coherent with practical experience.

In this paper, a two-phase decoupled framework was proposed such that sample size independence is enforced explic-

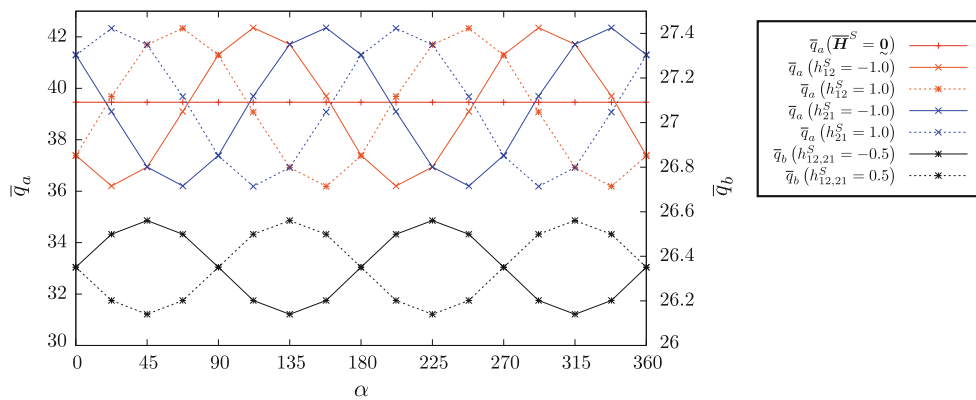


Fig. 16 Anisotropic flow behaviour for surfacial shearing with $\bar{v} = 0$ mm/s, $\bar{g} = 0.1$ MPa/mm. Quantities denoted by \bar{q}_a refer to the left axis and \bar{q}_b refer to the right axis, respectively

ity. The sample size effect is the subject of investigation in [11]. Here, the comparison of a fully coupled framework with the decoupled setting reveals a significant deviation when the length scale separation assumption is violated. The consistent incorporation of the coupled framework into a macroscopic lubrication formulation that can display such size effects remains as a future investigation.

A validation with experimental results should be conducted but would be premature due to several omitted effects which should be explored for the finite deformation regime. Throughout the interface effects like temperature dependence, asperity deformation induced by surface shearing and hence the lubricant tangential friction are present. Furthermore, the REYNOLDS equation will be violated for increasing amplitudes or little gap heights such that STOKES equation needs to be solved. The contact of the adjacent surfaces would complete the present investigations on simple surface geometries, but real roughness profiles also need to be investigated. Due to the random characteristics of real surfaces, sample size effects would play a role. Randomness effects can be alleviated by complementing surface averaging with ensemble averaging combined with sample enlargement, albeit at the expense of high computational cost. However it is expected that optimal computational efficiency will be retained due to the decoupled framework. Finally, a key future investigation is the realization of the coupling to the macroscale by means of numerical tangent computations enabling the use of implicit solution schemes and hence a reduction of computational cost.

Acknowledgments This work has been funded by a German Research Foundation grant (within DFG/GRK615).

References

- Almqvist A, Dasht J (2006) The homogenization process of the Reynolds equation describing compressible liquid flow. *Tribol Int* 39:994–1002
- Almqvist A, Essel E, Fabricius J, Wall P (2008) Reiterated homogenization applied in hydrodynamic lubrication. *Proc Inst Mech Eng Part J J Eng Tribol* 222(7):827–841
- Almqvist A, Essel E, Persson L, Wall P (2007) Homogenization of the unstationary incompressible Reynolds equation. *Tribol Int* 40(9):1344–1350
- Almqvist A, Lukkassen D, Meidell A, Wall P (2007) New concepts of homogenization applied in rough surface hydrodynamic lubrication. *Int J Eng Sci* 45(1):139–154
- Bakhvalov N, Panasenko G (1989) *Homogenisation: averaging processes in periodic media*. Kluwer, Dordrecht
- Bayada G, Chambat M (1989) Homogenization of the Stokes system in a thin film flow with rapidly varying thickness. *Modélisation mathématique et analyse numérique* 23(2):205–234
- Bayada G, Martin S, Vázquez C (2005) An average flow model of the Reynolds roughness including a mass-flow preserving cavitation model. *J Tribol* 127:793–802
- Bayada G, Martin S, Vázquez C (2006) Micro-roughness effects in (elasto) hydrodynamic lubrication including a mass-flow preserving cavitation model. *Tribol Int* 39(12):1707–1718
- Bensoussan A, Lions JL, Papanicolaou G (1978) *Asymptotic analysis for periodic structures*. North-Holland, Amsterdam
- Bohan M, Fox I, Claypole T, Gethin D (2003) Influence of non-Newtonian fluids on the performance of a soft elastohydrodynamic lubrication contact with surface roughness. *Proc Inst Mech Eng Part J J Eng Tribol* 217(6):447–459
- Budt M (2012) *Computational homogenization framework for soft elasto-hydrodynamic lubrication*. PhD thesis, Institut für Kontinuumsmechanik, Gottfried Wilhelm Leibniz Universität Hannover, Hannover (Germany)
- Buscaglia G, Ciuperca I, Jai M (2007) On the optimization of surface textures for lubricated contacts. *J Math Anal Appl* 335(2):1309–1327
- Charnes A, Osterle F, Saibel E (1952) On the energy equation for fluid-film lubrication. *Proc R Soc Lond Ser A Math Phys Sci* 214:133–136
- Cope W (1949) The hydrodynamical theory of film lubrication. *Proc R Soc Lond Ser A Math Phys Sci* 197(1049):201–217
- Curnier A, Taylor RL (1982) A thermomechanical formulation and solution of lubricated contacts between deformable solids. *J Lubr Technol* 104:109–117
- de Kraker A, van Ostayen RAJ, Rixen DJ (2010) Development of a texture averaged Reynolds equation. *Tribol Int* 43:2100–2109
- Dowson D (1995) Elastohydrodynamic and micro-elastohydrodynamic lubrication. *Wear* 190(2):125–138

18. Elrod H (1979) A general theory for laminar lubrication with Reynolds roughness. *ASME Trans J Lubr Technol* 101:8–14
19. Ervin RD, Balderas L (1990) Hydroplaning with lightly-loaded truck tires. Technical Report UMTRI-90-6, Transportation Research Institute, The University of Michigan
20. Fabricius J (2008) Homogenization theory with applications in tribology. PhD thesis, Luleå University of Technology
21. Fung YC (1993) *Biomechanics: mechanical properties of living tissues*, 2nd edn. Springer, New York
22. Hamrock B, Schmid S, Jacobson B (2004) *Fundamentals of fluid film lubrication*. CRC Press, Boca Raton
23. Huebner K (1975) *The finite element method for engineers*. Wiley-Interscience, New York
24. Jackson RL (2010) A scale dependent simulation of liquid lubricated textured surfaces. *J Tribol* 132:022001
25. Jaffar M (2000) A numerical solution for a soft line elastohydrodynamic lubrication contact problem with sinusoidal roughness using the Chebyshev polynomials. *Proc Inst Mech Eng Part C J Mech Eng Sci* 214(5):711–718
26. Jai M, Bou-Said B (2002) A comparison of homogenization and averaging techniques for the treatment of roughness in slip-flow-modified Reynolds equation. *J Tribol* 124:327
27. Kane M, Bou-Said B (2004) Comparison of homogenization and direct techniques for the treatment of roughness in incompressible lubrication. *J Tribol* 126:733
28. Kane M, Bou-Said B (2005) A study of roughness and non-newtonian effects in lubricated contacts. *J Tribol* 127:575
29. Kane M, Do T (2006) A contribution of elastohydrodynamic lubrication for estimation of tire-road friction in wet conditions. In: *Proceedings of the International Conference on Tribology, Parma, Italy, September 20–22 2006: AITC-AIT 2006*
30. Larsson R (2009) Modelling the effect of surface roughness on lubrication in all regimes. *Tribol Int* 42(4):512–516
31. Lewis R, Gallardo-Hernandez EA, Hilton T, Armitage T (2009) Effect of oil and water mixtures on adhesion in the wheel/rail contact. *Proc IMechE Part F J Rail Rapid Transit* 223:275–283
32. Lukkassen D, Meidell A, Wall P (2007) Bounds on the effective behavior of a homogenized generalized Reynolds equation. *J Funct Spaces Appl* 5:133–150
33. Mitsuya Y, Fukui S (1986) Stokes roughness effects on hydrodynamic lubrication. Part I—comparison between incompressible and compressible lubricating films. *J Tribol* 108:151
34. Patir N, Cheng H (1978) An average flow model for determining effects of three-dimensional roughness on partial hydrodynamic lubrication. *ASME Trans J Lubr Technol* 100:12–17
35. Patir N, Cheng H (1979) Application of average flow model to lubrication between rough sliding surfaces. *ASME J Lubr Technol* 101(2):220–230
36. Persson B (2000) *Sliding friction: physical principles and applications*, vol 1. Springer, Berlin
37. Persson BNJ (2010) Fluid dynamics at the interface between contacting elastic solids with randomly rough surfaces. *J Phys Condens Matter* 22:265004
38. Rabinowicz E (1995) *Friction and wear of materials*, 2nd edn. Wiley, New York
39. Rajagopal K, Szeri A (2003) On an inconsistency in the derivation of the equations of elastohydrodynamic lubrication. *Proc R Soc Lond Ser A Math Phys Eng Sci* 459(2039):2771
40. Reynolds O (1886) On the theory of lubrication and its application to Mr. Beauchamp tower's experiments, including an experimental determination of the viscosity of olive oil. *Philos Trans R Soc Lond* 177:157–234
41. Sahlin F, Almqvist A, Larsson R, Glavatskih S (2007) Rough surface flow factors in full film lubrication based on a homogenization technique. *Tribol Int* 40(7):1025–1034
42. Sahlin F, Larsson R, Almqvist A, Lugt P, Marklund P (2010a) A mixed lubrication model incorporating measured surface topography. Part 1: theory of flow factors. *Proc Inst Mech Eng Part J J Eng Tribol* 224(4):335–351
43. Sahlin F, Larsson R, Marklund P, Almqvist A, Lugt P (2010b) A mixed lubrication model incorporating measured surface topography. Part 2: roughness treatment, model validation, and simulation. *Proc Inst Mech Eng Part J J Eng Tribol* 224(4):353–365
44. Sanchez-Palencia E (1980) *Non-homogeneous media and vibration theory*. Springer, Berlin
45. Shi F, Salant R (2000) A mixed soft elastohydrodynamic lubrication model with interasperity cavitation and surface shear deformation. *J Tribol* 122(1):308–316
46. Shinkarenko A, Kligerman Y, Etsion I (2009) The validity of linear elasticity in analyzing surface texturing effect for elastohydrodynamic lubrication. *J Tribol* 131:021503
47. Shukla J (1978) A new theory of lubrication for rough surfaces. *Wear* 49(1):33–42
48. Stachowiak G, Batchelor A (2005) *Engineering tribology*. Butterworth-Heinemann, Boston
49. Stupkiewicz S (2007) *Micromechanics of contact and interphase layers micromechanics of contact and interphase layers*. Springer, Berlin
50. Stupkiewicz S, Maciniszyn A (2004) Modelling of asperity deformation in the thin-film hydrodynamic lubrication regime. In: *Proceedings of the 2nd international conference on tribology in manufacturing processes, Nyborg, Denmark, June 15–18, 2004: ICTMP2004*, 695p
51. Szeri AZ (2011) *Fluid film lubrication*, 2nd edn. Cambridge University Press, Cambridge
52. Tala-Ighil N, Fillon M, Maspeyrot P (2011) Effect of textured area on the performances of a hydrodynamic journal bearing. *Tribol Int* 44:211–219
53. Temizer İ (2011) Thermomechanical contact homogenization with random rough surfaces and microscopic contact resistance. *Tribol Int* 44(2):114–124
54. Temizer İ, Wriggers P (2010) Thermal contact conductance characterization via computational contact homogenization: a finite deformation theory framework. *Int J Numer Methods Eng* 83(1):27–58
55. Temizer İ, Wriggers P (2011) Homogenization in finite thermoelasticity. *J Mech Phys Solids* 59(2):344–372
56. Torquato S (2002) *Random heterogeneous materials: microstructure and macroscopic properties*. Springer, Berlin
57. Tripp J (1983) Surface roughness effects in hydrodynamic lubrication: the flow factor method. *J Lubr Technol* 105(3):458–465
58. Wagner W, Gruttmann F (1994) A simple finite rotation formulation for composite shell elements. *Eng Comput* 11(2):153–155
59. Walowit J, Anno J (1975) *Modern developments in lubrication mechanics*. Applied Science Publishers, London
60. Wriggers P (2006) *Computational contact mechanics*, 2nd edn. Springer, Berlin
61. Zohdi TI, Wriggers P (2008) An introduction to computational micromechanics, vol 20 of *Lecture Notes in Applied and Computational Mechanics*. Springer, Berlin